

Direct Observation of Momentum-Dependent Exchange Interaction in a Heisenberg Ferromagnet

H. Miyazaki,^{1,2,*} T. Ito,^{1,3} H. J. Im,^{1,4} S. Yagi,² M. Kato,² K. Soda,^{2,1} and S. Kimura^{1,3,†}

¹*UVSOR Facility, Institute for Molecular Science, Okazaki 444-8585, Japan*

²*Graduate School of Engineering, Nagoya University, Nagoya 464-8603, Japan*

³*School of Physical Sciences, The Graduate University for Advanced Studies (SOKENDAI), Okazaki 444-8585, Japan*

⁴*Department of Physics, Sungkyunkwan University, Suwon 440-749, South Korea*

(Received 3 December 2008; published 5 June 2009)

We measured the temperature-dependent three-dimensional angle-resolved photoemission spectra of EuO (100) thin film, a typical Heisenberg ferromagnetic semiconductor, to investigate the essential origin of the ferromagnetic transition. We observed sizable energy dispersion and large binding-energy shift of the Eu 4*f* state below the Curie temperature only near the Γ and *X* points, despite the expected Heisenberg-type local magnetism. The band dispersion and temperature dependence of the Eu 4*f* state indicates that the indirect exchange and superexchange interactions have strong momentum dependence. The observed temperature-dependent energy shift of the 4*f* state is the essential origin of the magnetism of EuO.

DOI: [10.1103/PhysRevLett.102.227203](https://doi.org/10.1103/PhysRevLett.102.227203)

PACS numbers: 75.50.Pp, 75.70.Ak, 79.60.-i

Local magnetism is generally believed to originate from the direct interaction among isolated electron spins described by the Heisenberg model with the Hamiltonian, $H = -\sum_{i,j} J_{i,j} \vec{S}_i \cdot \vec{S}_j$, in which the electronic states with local magnetic moments are perfectly localized [1]. In rare-earth compounds, instead of direct exchange interaction, superexchange interaction mediated by ligand valence electrons and indirect exchange interaction by conduction electrons among rare-earth ions are dominant because the 4*f* state in rare-earth ions is spatially localized. In the case of the superexchange and indirect exchange interactions, hybridization between the 4*f* electrons with local magnetic moments and the valence/conduction electrons is important. However, no direct observation of this phenomenon has been performed so far.

Europium chalcogenides (EuX; X = O, S, Se, Te) have long been known as typical Heisenberg magnets with Eu²⁺ 4*f* local moments. Among them, EuO is a ferromagnetic material with a Curie temperature (T_C) of about 70 K [2–4]. The magnetic properties have been explained by a Heisenberg model, because its magnetic moment of $6.9\mu_B$ is similar to that of a free Eu²⁺ ion. According to the Heisenberg model, where Eu 4*f* electrons are treated as localized spins, ferromagnetic transition is triggered by exchange interactions of the Eu 4*f* electrons through virtual 4*f* transitions to the unoccupied Eu 5*d* conduction state and to the occupied O 2*p* valence state, originating in the indirect exchange and superexchange interaction, respectively [4–6]. On the other hand, in most 4*f* electron systems, anomalous electronic/magnetic properties, especially the coexistence of superconductivity and magnetism, have been attributed to the character of 4*f* electrons (localized or itinerant). Furthermore, the existence of Ce 4*f* band dispersion in heavy-fermion systems has been inves-

tigated by resonant angle-resolved photoemission spectroscopy, with the results indicating the importance of momentum-dependent hybridization between the 4*f* and itinerant conduction electrons as a perspective for understanding the essential origin of anomalous properties in 4*f* electron systems [7].

To date, changes in the electronic structure of EuO at T_C have been investigated using infrared [8–11], x-ray adsorption [12], and angle-integrated photoemission spectroscopy [13–17]. Although the obtained data show the change in the electronic structure caused by magnetic ordering, the change in the band structure to clarify the momentum dependence of the 4*f* state and its relation to the exchange interaction have never been investigated.

In this Letter, we describe a study in which we measured the three-dimensional angle-resolved photoemission spectra [3D angle-resolved photoemission spectroscopy (ARPES)] of a single-crystalline EuO thin film to investigate the essential origin of the ferromagnetic transition as well as the character of Eu 4*f* electrons. We found clear energy dispersion of the Eu 4*f* state across T_C . The Eu 4*f* bands show two types of energy shift below T_C : one in which the overall electronic structure shifts to the lower binding-energy side, and the other in which the Eu 4*f* majority-spin bands and O 2*p* majority-spin bands shift away from each other only near the Γ and *X* points. While the former originates from band splitting between the majority and minority spins in the ferromagnetic phase, the latter can be attributed to strong hybridization between the Eu 4*f* and O 2*p* states. Furthermore, the energy shift of the Eu 4*f* bands at the *X* point (≤ 0.1 eV) is much smaller than that at the Γ point (~ 0.3 eV), due to strong Eu 4*f*–5*d* hybridization. These results, indicating the hybridizations of Eu 4*f*–O 2*p* and Eu 4*f*–5*d* corresponding to the momentum-dependent superexchange and indirect ex-

change interactions, respectively, have been directly observed for the first time.

Single-crystalline EuO thin films with a thickness of about 50 nm were fabricated using the molecular beam epitaxy method [18]. As shown in Fig. 1(a), epitaxial growth of the single-crystalline EuO thin films by 1×1 EuO (100) patterns was confirmed with low energy electron diffraction. Layer-by-layer growth of EuO has been confirmed by reflection high energy electron diffraction, as well. The value of T_C measured with a superconducting quantum interference device magnetometer was 71 K, which is slightly higher than the ordering temperature of the bulk EuO. The 3D ARPES measurements were performed at the beam line 5U of UVSOR-II [19], the Institute for Molecular Science, combined with the molecular beam epitaxy system. As shown in Fig. 1(b), the Γ and X points in the normal emission geometry correspond to the photon energy $h\nu$ of 78 and 38 eV; these values were determined experimentally from the photon-energy dependence of the normal emission 3D ARPES spectra [20]. The total energy and momentum resolutions of the present 3D ARPES measurements were set to 123 meV (45 meV) and 0.020 \AA^{-1} (0.014 \AA^{-1}) at the Γ (X) point, respectively. The Fermi energy (E_F) was determined by measuring the evaporated gold film spectra.

Figures 2(g1)–2(g3), and 2(x1)–2(x3) show the 3D ARPES results for EuO (100) near the Γ and X points, respectively. Representative 3D ARPES images of paramagnetic [Figs. 2(g2) and 2(x2)] and ferromagnetic [Figs. 2(g3) and 2(x3)] EuO were plotted at 5 and 120 K, respectively. The local minimums on the second-derivative energy distribution curves (EDCs) indicate the peaks (shoulders) of the EDCs as shown in Figs. 2(g1) and 2(x1). The bright areas and open circles indicating the second-derivative peaks correspond to the band dispersion as shown in Figs. 2(g2), 2(g3), 2(x2), and 2(x3). Figures 2(g4) and 2(x4) show the band structure near the Γ and X points, respectively, in the ferromagnetic phase [20] calculated by a spin-polarized full potential linearized augmented plane wave using the on-site Coulomb interaction [local spin density plus Coulomb repulsion U (LSDA + U) method] implemented in the WIEN2K code

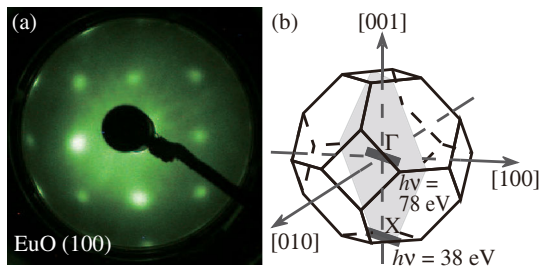


FIG. 1 (color online). (a) Low energy electron diffraction pattern of EuO (100) thin film. (b) The first Brillouin zone and the high-symmetry points. The photon energies corresponding to the Γ and X points in the normal emission geometry are denoted.

[21]. From a comparison with the band calculation, the experimental bands observed at a binding energy E_B of 1.0–3.5 eV and 4.0–7.0 eV are attributed to the Eu 4*f* and O 2*p* states, respectively. This assignment is consistent with the photoionization cross section [22], which reduces the Eu 4*f*/O 2*p* spectral weight ratio from $h\nu = 78$ to 38 eV [see Figs. 2(g1) and 2(x1)]. Furthermore, the observed dispersive features of the Eu 4*f* state are well reproduced by the band calculation in the ferromagnetic phase. For example, there are three (two) Eu 4*f* bands at the Γ (X) point and one of those near E_F disperses to the higher binding-energy side and merges into the nondispersive partner away from the Γ (X) point. The splitting energy of the O 2*p* state is consistent with the band calculation in Figs. 2(g4) and 2(x4), and also with the spin-resolved photoemission spectroscopy results [17]. Here, the O 2*p* bands at the higher and lower binding energies are attributed to the majority- and minority-spin states, respectively.

In the Heisenberg model the Eu 4*f* state is expected to be fully localized and to have no energy dispersion. However, we clearly observed sizeable energy dispersion of the Eu 4*f* state in both the para- and ferromagnetic phases. To clarify the essential origin of ferromagnetic transition, we measured the temperature dependence of the 3D ARPES spectrum across T_C . Figures 3(g1) [3(g2)]

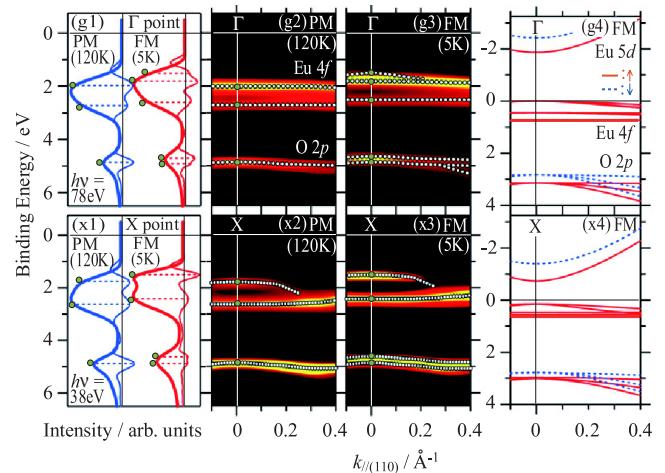


FIG. 2 (color online). Energy distribution curves (EDCs, thick lines) and their second-derivative EDCs (thin lines) of EuO (100) thin film in the paramagnetic phase (PM) at 120 K and in the ferromagnetic phase (FM) at 5 K at the Γ (g1) and X (x1) points. The dashed lines indicate the peaks in the second-derivative EDCs that correspond to the peaks and shoulders in the EDCs. The 3D ARPES images were derived from the second-derivative EDCs in the paramagnetic phase at 120 K and in the ferromagnetic phase at 5 K near the Γ [(g2), (g3)] and X [(x2), (x3)] points. The open circles in (g2), (g3), (x2), and (x3) indicate the peaks and shoulders in the 3D ARPES images. The band structures calculated by the LSDA + U ($U = 7$ eV) method are shown near the Γ (g4) and X (x4) points. The solid and dashed lines in (g4) and (x4) denote the majority (\uparrow) and minority (\downarrow) spin states, respectively.

and 3(x1) [3(x2)] show the temperature dependence of the Eu 4*f* [O 2*p*] band at the Γ and *X* points, respectively. The circles and bright areas correspond to the peak positions of the second-derivative EDCs. With decreasing temperature across T_C , all of the bands shift by 0.2–0.3 eV to the lower binding-energy side. The overall energy shift is in good agreement with the magnetic red shift estimated from the optical absorption spectra [8–11]. This indicates that the overall energy shift originates from the changing of the bottom energy of the Eu 5*d* conduction band at the *X* point due to the energy gain of the Eu 5*d* majority-spin state after band splitting caused by ferromagnetic ordering. In other words, E_F is located at the bottom of the Eu 5*d* state. This is supported by the fact that the overall band shift (0.2–0.3 eV) is found to be half the exchange splitting energy of the Eu 5*d* state (0.5–0.6 eV) at the *X* point by the band calculation [see Fig. 2(x4)].

To explore the momentum-dependent component from the temperature-dependent hybridization effect between the Eu 4*f* and O 2*p* states and between the Eu 4*f* and Eu 5*d* states, we set the nonbonding Eu 4*f* state at 2.7 eV at the Γ point in Fig. 3(g1) so as to be fixed with the temperature. The nonbonding Eu 4*f* state corresponds to the calculated Eu 4*f* band at 0.8 eV (thick line) in Figs. 2(g4) and 2(x4). After the reference point is set to the nonbonding Eu 4*f* state, the temperature dependence of the Eu 4*f* and O 2*p* bands at the Γ and *X* points due to the momentum-dependent component appears as shown in Fig. 4. The figure depicts the temperature-dependent energy shift of the bottom of the Eu 5*d* band at the *X* point, which is consistent with the temperature dependence of the binding energy of the nonbonding Eu 4*f* state as shown in Fig. 4(x0). Using this methodology, we can clearly see the momentum-dependent energy shift of the Eu 4*f*, Eu 5*d*,

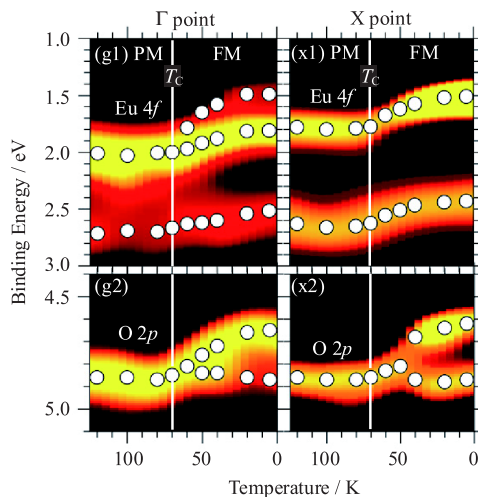


FIG. 3 (color online). Temperature dependence of the photoemission peak energies derived from the second-derivative EDCs of the Eu 4*f* [(g1), (x1)] and O 2*p* [(g2), (x2)] states at the Γ and *X* points. The open circles indicate the peaks of the second-derivative EDCs.

and O 2*p* bands through the ferromagnetic transition. For example, the top of the Eu 4*f* band and the bottom of the O 2*p* band shift to the lower and higher relative binding-energy sides, respectively, as a function of temperature. The observed energy shifts indicate the strong hybridization between the Eu 4*f* majority-spin and O 2*p* majority-spin bands below T_C , since the bonding and antibonding bands shift away from each other through the hybridization. The energy shift of the O 2*p* majority [minority] state at the Γ point [210 meV (–10 meV)] is almost the same as that at the *X* point [210 meV (–40 meV)]. In contrast, the energy shift of the Eu 4*f* band at the *X* point (70 meV) is smaller than that at the Γ point (320 meV). According to the band structure calculation, the bottom of the Eu 5*d* conduction bands is located at the *X* point, while the Eu 5*d* state at the Γ point is relatively far from the Eu 4*f* bands. Therefore, the Eu 4*f*–5*d* hybridization intensity at the *X* point is anticipated to be higher than that at the Γ point. Since the top of the Eu 4*f* band at the *X* point is located at a higher binding-energy side than that at the Γ point, the Eu 4*f*–5*d* hybridization operates in this system; i.e., the Eu 4*f* band at the *X* point is pushed down by the Eu 4*f*–5*d* hybridization. This is evidence for the indirect exchange interaction between the Eu 4*f* and 5*d* states.

Next we discuss the exchange interactions from the present 3D ARPES observations. Although the exchange interaction of EuO has been described by a Heisenberg model where Eu 4*f* electrons are treated as localized spins,

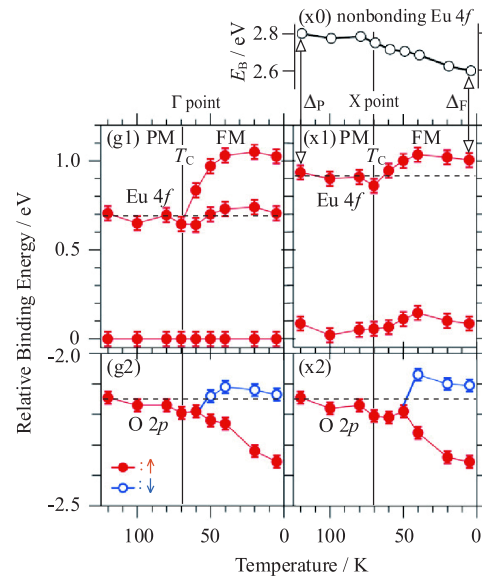


FIG. 4 (color online). Temperature dependence of the peak energies of the Eu 4*f* [(g1), (x1)] and O 2*p* [(g2), (x2)] states at the Γ and *X* points subtracted from the binding energy of the nonbonding Eu 4*f* state at a binding energy of 2.5–3 eV in Figs. 3(g1) and 3(x1). The upper panel (x0) shows the temperature dependence of the binding energy of the nonbonding Eu 4*f* state, which can be regarded as the temperature dependence of the bottom energy of the Eu 5*d* band. The energy gaps above and below T_C correspond to Δ_P and Δ_F , respectively.

it is also worthwhile applying this description to the momentum-dependent hybridization effect. There are two types of exchange interactions in EuO. One is the indirect exchange interaction, in which $4f$ spins involve a virtual excitation of the Eu $5d$ band. The other is the superexchange interaction, in which Eu $4f$ electrons are mediated via O $2p$ orbitals. From the electronic structure point of view, roughly speaking, the former can be attributed to the Eu $4f$ - $5d$, and the latter to the Eu $4f$ -O $2p$ hybridization effect. In other words, a different hybridization process causes a different exchange path in the ferromagnetic electronic structure. Here, we again focus on the obvious difference of the momentum-dependent hybridization effect across T_C . At the Γ point, we find a strong Eu $4f$ -O $2p$ hybridization effect relating to the superexchange interaction. On the other hand, at the X point, the Eu $5d$ electrons affect the Eu $4f$ bands via the Eu $5d$ -O $2p$ hybridization effect, competing with the Eu $4f$ -O $2p$ hybridization effect. Since the energy levels of the O $2p$ and Eu $5d$ states are well separated, the additional Eu $5d$ electron effect can be assigned as the Eu $4f$ - $5d$ hybridization process, which dominates the indirect exchange interaction as already discussed. The above assignment suggests that the indirect exchange interaction can be extracted from the superexchange Eu $4f$ -O $2p$ interaction since the Eu $4f$ -O $2p$ hybridization intensity at the Γ point should be similar to that at the X point. Although quantitative analysis of the exchange interaction requires extensive 3D ARPES data in the three-dimensional Brillouin zone, the present 3D ARPES observation of the temperature- and momentum-dependent hybridization effect across T_C indicates that the exchange interaction has momentum dependence in EuO.

The energy shifts of the Eu $4f$ state are about 320 ± 20 meV ($(37 \pm 2.3) \times 10^2$ K) at the Γ point and about 70 ± 20 meV ($(8.1 \pm 2.3) \times 10^2$ K) at the X point, which are several orders of magnitude higher than T_C . The error bar is attributed to the energy step of the ARPES spectra. If the energy shifts are assumed to occur in the local spherical area at the Γ and X points, the energy gain (ΔE) averaged in the first Brillouin zone can be evaluated using the following function:

$$\Delta E = \frac{1}{V_k} \left[\int_{\text{BZ}} \{E_{\text{ferro}}(k) - E_{\text{para}}(k)\} 4\pi k^2 dk \right],$$

where V_k is the volume of the first Brillouin zone (3.64 \AA^{-3}), $E_{\text{ferro}}(k)$ and $E_{\text{para}}(k)$ are the dispersion curves of the top of the Eu $4f$ band in the ferromagnetic and paramagnetic phases, respectively, observed in Figs. 4. The integration is done in the whole first Brillouin zone. When we consider that the temperature-dependent area is only about 1% (5%) near the Γ (X) point in the whole Brillouin zone, ΔE becomes about 82 ± 20 K, which is consistent with T_C . This indicates that the observed $4f$ band shifts at the high-symmetry points are important in the ferromagnetic phase transition of EuO. In other words, the momentum dependence of the hybridization as well as that of the

exchange interaction plays an important role, even in the typical Heisenberg-type magnetic material EuO.

In conclusion, we measured the temperature dependence of the 3D ARPES spectra of single-crystalline EuO (100) thin film. The peak energies of the Eu $4f$ and O $2p$ states at the Γ and X points drastically change across T_C . The band shifts can be attributed to the hybridization effects between the Eu $4f$ and O $2p$ states (superexchange interaction) and between the Eu $4f$ and $5d$ states (indirect exchange interaction). The band dispersions of the Eu $4f$ state due to the hybridization effect appear only near the Γ and X points, which causes the momentum-dependent exchange interaction in EuO. The momentum dependence of the interaction is important even in the typical Heisenberg-type ferromagnetic semiconductor EuO. The present observation will give us a chance to see deep insight into the mechanism of magnetic phase transition from an electronic structure perspective in the future.

We would like to thank Professor Sakai for his useful discussion. This work was performed a joint studies program of the Institute for Molecular Science (2007) and was partly supported by a Grant-in-Aid for Scientific Research (B) (No. 18340110) from the MEXT of Japan.

*hmiyazak@ims.ac.jp

†kimura@ims.ac.jp

- [1] N. W. Ashcroft and N. D. Mermin, *Solid State Physics* (Saunders College, Philadelphia, 1976).
- [2] B. Matthias, R. Bozorth, and J. V. Vleck, Phys. Rev. Lett. **7**, 160 (1961).
- [3] N. Tsuda *et al.*, *Electronic Conduction in Oxides*, Springer Series in Solid-State Sciences (Springer, New York, 2000).
- [4] N. Mauger *et al.*, J. Phys. (Paris) **39**, 1125 (1978).
- [5] T. Kasuya *et al.*, IBM J. Res. Dev. **14**, 214 (1970).
- [6] A. Mauger and C. Godart, Phys. Rep. **141**, 51 (1986).
- [7] H. J. Im *et al.*, Phys. Rev. Lett. **100**, 176402 (2008).
- [8] G. Busch, P. Junod, and P. Wachter, Phys. Lett. **12**, 11 (1964).
- [9] M. J. Freiser *et al.*, Helv. Phys. Acta **41**, 832 (1982).
- [10] J. Schoenes and P. Wachter, Phys. Rev. B **9**, 3097 (1974).
- [11] S. Kimura *et al.*, Phys. Rev. B **78**, 052409 (2008).
- [12] P. G. Steeneken *et al.*, Phys. Rev. Lett. **88**, 047201 (2002).
- [13] D. E. Eastman, F. Holtzberg, and S. Methfessel, Phys. Rev. Lett. **23**, 226 (1969).
- [14] G. Busch, P. Cotti, and P. Munz, Solid State Commun. **7**, 795 (1969).
- [15] D. E. Eastman and M. Kuznietz, J. Appl. Phys. **42**, 1396 (1971).
- [16] P. Cotti and P. Munz, Helv. Phys. Acta **45**, 19 (1972).
- [17] H. Lee *et al.*, J. Appl. Phys. **102**, 053903 (2007).
- [18] H. Miyazaki *et al.*, Jpn. J. Appl. Phys. (to be published).
- [19] T. Ito *et al.*, AIP Conf. Proc. **879**, 587 (2007).
- [20] H. Miyazaki *et al.*, Physica B (Amsterdam) **403**, 917 (2008).
- [21] P. Blaha *et al.*, Comput. Phys. Commun. **59**, 399 (1990).
- [22] J. J. Yeh and I. Lindau, At. Data Nucl. Data Tables **32**, 1 (1985).